ADVANCED INTELLIGENT SYSTEMS
Open Access
www.advintellsyst.com

Piezo Capsule: Ultrasonic Way of Wireless Pressure Measurement

*Senol Mutlu, Amirreza Aghakhani, and Metin Sitti**

Heart failure (HF) rates elevate worldwide with the aging population. Miniaturized and wireless implants with real-time data transfer capability can alleviate the surgical complexities of cardiac pressure monitoring. Despite recent developments of mm-size implants with complex circuitries and self-powering units, a simple, passive, and effective implant design for the real-time pressure reading is missing. Here, the piezo capsule, a simple, cost-effective, and miniaturized passive ultrasound pressure sensing system, is introduced. The capsule design consists of a 1 mm-cube-sized lead zirconate titanate (PZT) transducer and a T-shaped mechanical pin. The impedance changes of an interrogating ultrasound probe, which is ultrasonically coupled to the receiver implant, correlate to the electrical/mechanical loading of the piezo capsule. The ultrasonic sensing properties of the proposed device are characterized across a hard-solid medium (e.g., plexiglass) and soft tissue-like media (e.g., polydimethylsiloxane (PDMS) and chicken breast tissue) and verified the impedance changes using finite element simulations. Last, dynamic wireless pressure readings of an artificial vessel for varying fluid flow pulse-frequency and volumetric rate are demonstrated. The sensitivity of 0.375 $\Omega\,kPa^{-1}$ is achieved as the pressure changed from 14 to 86 kPa and pulse frequency from 0 to 100 bpm with a fixed flow rate of 8 $mL\,min^{-1}$.

1. Introduction

Heart failure (HF) is the inability of the heart to provide adequate blood flow to the body, affecting around 26 million people worldwide, which increases with the aging population.[1] Pulmonary arterial pressure values are often used to diagnose heart failure conditions first and then to monitor them. These measurements are often done in uncomfortable and expensive clinic visits.[2] Alternative health management strategies are needed to extend and improve the quality of life for HF patients at an affordable cost. Permanent implants with real-time intracardiac hemodynamic monitoring capability under ambulatory conditions offer viable solutions and can provide personalized and cost-effective care.[3] Miniaturization and wireless operation are key requirements for the successful deployment of these implants in clinical applications.[4]

In the absence of wireless operation, transdermal or percutaneous wires become the primary sources of infection, failure, manufacturing cost, and discomfort to the patient.[5] The battery is also not a preferred option since it puts a limit on the overall size of the implant and shortens its lifetime. Miniaturization of implants is necessary to reduce their adverse impacts on the body, e.g., blocking any artery flow[6] or giving discomfort to the patient. In the future, it would become imperative to record pressure values from multiple sites of the heart and arteries to detect other pathologies or to use ventricular assist pumps.[3] Hence, small volumes (less than 1 mm^3), independent, free-floating, and wireless pressure sensor modules in large quantities are much needed for HF patients. Sufficient wireless operation distances with small volumes without violating the specific absorption rate (SAR) limits are the stringent constraints,[7] which must be overcome.

For this purpose, wireless power transmission (WPT) and energy harvesting technologies have been extensively studied for implantable medical devices. Radiofrequency (RF), mostly inductive coupling,[5,8,9] ultrasonic,[10–14] optical,[15–17] electrostatic,[18,19] electromagnetic,[20–23] thermoelectric,[24] and

S. Mutlu, A. Aghakhani, M. Sitti
Physical Intelligence Department
Max Planck Institute for Intelligent Systems
Stuttgart 70569, Germany
E-mail: sitti@is.mpg.de

The ORCID identification number(s) for the author(s) of this article can be found under https://doi.org/10.1002/aisy.202200125.

© 2022 The Authors. Advanced Intelligent Systems published by Wiley-VCH GmbH. This is an open access article under the terms of the Creative Commons Attribution License, which permits use, distribution and reproduction in any medium, provided the original work is properly cited.

DOI: 10.1002/aisy.202200125

S. Mutlu
Department of Electrical and Electronics Engineering
Bogazici University
Istanbul 34342, Turkey

M. Sitti
School of Medicine and School of Engineering
Koc University
Istanbul, Turkey

M. Sitti
Institute for Biomedical Engineering
ETH Zurich
Zurich, Switzerland

26404567, 2022, 10, Downloaded from https://onlinelibrary.wiley.com/doi/10.1002/aisy.202200125 by Koc University, Wiley Online Library on [03/11/2022]. See the Terms and Conditions (https://onlinelibrary.wiley.com/terms-and-conditions) on Wiley Online Library for rules of use; OA articles are governed by the applicable Creative Commons License

26404567, 2022, 10, Downloaded from https://onlinelibrary.wiley.com/doi/10.1002/aisy.202200125 by Koc University, Wiley Online Library on [03/11/2022]. See the Terms and Conditions (https://onlinelibrary.wiley.com/terms-and-conditions) on Wiley Online Library for rules of use; OA articles are governed by the applicable Creative Commons License

triboelectric[25–28] methods have been investigated. Among these, RF and ultrasonic methods have emerged as viable solutions to overcome the long operation range and low power density constraints of miniaturized wireless sensory implants.[2,3,29–33]

RF methods in the form of two closely coupled coils have shown successful clinical results. For instance, CardioMEMS is an RF-based wireless blood pressure sensor that utilizes a hermetically sealed resonant circuit of an inductor coil and a micro-electro-mechanical system (MEMS) based capacitive pressure sensor.[30] It works over a distance of 20 cm with a size of $3.5 \times 2 \times 15\ mm^3$ and is implanted in increasing numbers of HF patients with high success.[34] Another wireless and batteryless implantable hemodynamic monitor system, called Titan, has been developed for long-term monitoring of cardiac function which comprises a MEMS pressure sensor, application-specific integrated circuit (ASIC), and a telemetry antenna for RF communication with an 18 mm overall size.[3,29] In general, RF systems require large coil sizes for operation because of the MHz radiofrequency range. Typically, the low-MHz region from 3 to 30 MHz is a good compromise between tissue absorption losses and coil size.[9] Downscaling the coil size to the millimeter range can only be achieved using the GHz frequency range with the cost of larger tissue path losses[35] and design complexity.[36–39] Regulations also put stringent limitations on the maximum possible transmitted RF power to biomedical implants, e.g., $1\ mW\ cm^{-2}$ power densities for frequencies from 100 to 300 MHz.[40] To overcome these shortcomings, ultrasonic WPT has been leveraged as a viable alternative to power and communicate with sub-mm-sized implants in the human body.[39]

Ultrasonic WPT offers smaller power losses through the human body, compared to the RF one. As a comparison, ultrasound power transfer through a brain tissue of 2 mm thickness results in only 1 dB attenuation at a wavelength of 150 μm (10 MHz), whereas an RF WPT with a wavelength of 5 mm (10 GHz) results in 20 dB attenuation. The low sound wave velocity in tissue allows ultrasonic operation at dramatically lower frequencies of around 1 MHz for miniaturized sensory implants with sizes less than 1 mm.[11,41] Moreover, according to Food and Drug Administration (FDA) regulations, the maximum allowed derated spatial peak temporal-average intensity ($I_{SPTA.3}$) of acoustic exposure is $430\ mW\ cm^{-2}$ for cardiac use,[42] which is much larger than what is allowed for RF WPT.

Recent developments of ultrasonically powered miniaturized wireless and batteryless implants include neural dust,[10,43] active implantable pressure sensor system,[44] and temperature sensor system.[14] Neural dust is an implantable neural stimulator that incorporates a piezoelectric transducer, an energy-storage capacitor, and ASIC in a $1.7\ mm^3$ volume, which may achieve a 70 mm working distance at 1.85 MHz.[43] A hand-held external piezoelectric transducer that is ultrasonically coupled to the piezoelectric transducer of the implant provides power and bidirectional communication with backscatter modulation, similar to passive radio frequency identification (RFID) tags.[10] Similar systems in the form of fully packaged miniature implants with ASIC, an energy storage capacitor, piezoelectric transducer, and a sensor node in the form of a pressure sensor[44] or temperature sensor[14] have been developed to work with ultrasonic data uplink. Efficient ultrasonic power links for sub-mm sized piezoelectric receivers have been shown to have link efficiencies of 1.93% and 0.23% at tissue depths of 6 and 10 cm, respectively, with an optimal carrier frequency range of around 1–2 MHz.[45] However, designing such miniature systems with ASICs that are low-power[46] and capable of communicating at distances of centimeters is challenging and needs high investments.[47] In contrast to the extensive and impressive research efforts on wireless ultrasonic miniaturized systems, no simple, cost-effective, and passive HF pressure sensing system, an alternative to RF ones, has been developed yet.

Here, we introduce the piezo capsule, a simple and passive wireless pressure sensing system for HF monitoring that uses a single 1 mm cube-sized lead zirconate titanate (PZT) transducer and a T-shaped mechanical pin. The key point of the implant design is the lack of complex electronics which facilitates the ease of use and reduces costs. Exploiting the physics of acoustic coupling between two piezoelectric elements, we could establish a real time, wireless dynamic pressure reading. The PZT material used in this work is an off-the-shelf product, known for its high piezoelectric coefficient.[41] Furthermore, using an integrated mechanical T-shaped design, we could amplify the pressure received on the PZT cube surface, leading to an enhanced acoustic coupling between the transmitter (TX) and receiver (RX).

The piezo capsule is ultrasonically coupled to an interrogating larger-sized, custom-made ultrasound probe which has the same resonant frequency as that of the piezo capsule (**Figure 1**A,B). This single piezo capsule enables wireless dynamic pressure readings as its resonance frequency and complex impedance change under mechanical loading, i.e., pressure. A novel T-shaped pin can focus the incident vessel pressure onto the piezo transducer, the effect of which can be ultrasonically picked up by the piezo probe. In this work, we first characterize the ultrasonic coupling of a $1\ mm^3$ piezo cube and its interrogating piezo probe across hard-solid and soft tissue-like media. Then, we demonstrate dynamic wireless pressure readings using the piezo capsule successfully embedded on a vessel-like polyurethane tube inside a bulk PDMS, mimicking body tissue. Using a pulsatile pump, we achieve a realistic pulsatile flow inside the artificial vessel and record the pressure amplitude via a reference wired pressure sensor. Simultaneously, the impedance analyzer recording of the interrogating piezo probe, which is ultrasonically coupled to the piezo capsule, shows a good correlation with the reference pressure profile for different volumetric flow rates and pulse frequencies. The simple, versatile, and passive piezo capsule proposed in this study could be used for long-term pressure reading in cardiac applications.

2. Results

2.1. Design and Working Principle of the Piezoelectric Capsule

The design concept of a piezoelectric capsule implant with an interrogating piezoelectric probe is shown in Figure 1A,B. The center axis of the piezo probe (TX) is aligned with the embedded piezo capsule (RX) to achieve optimum acoustic coupling. The front and backside electrodes of TX are connected to an impedance analyzer for monitoring and recording the amplitude and phase of the piezo probe's impedance in the frequency domain. The frequency-dependent impedance waveform of TX

© 2022 The Authors. Advanced Intelligent Systems published by Wiley-VCH GmbH

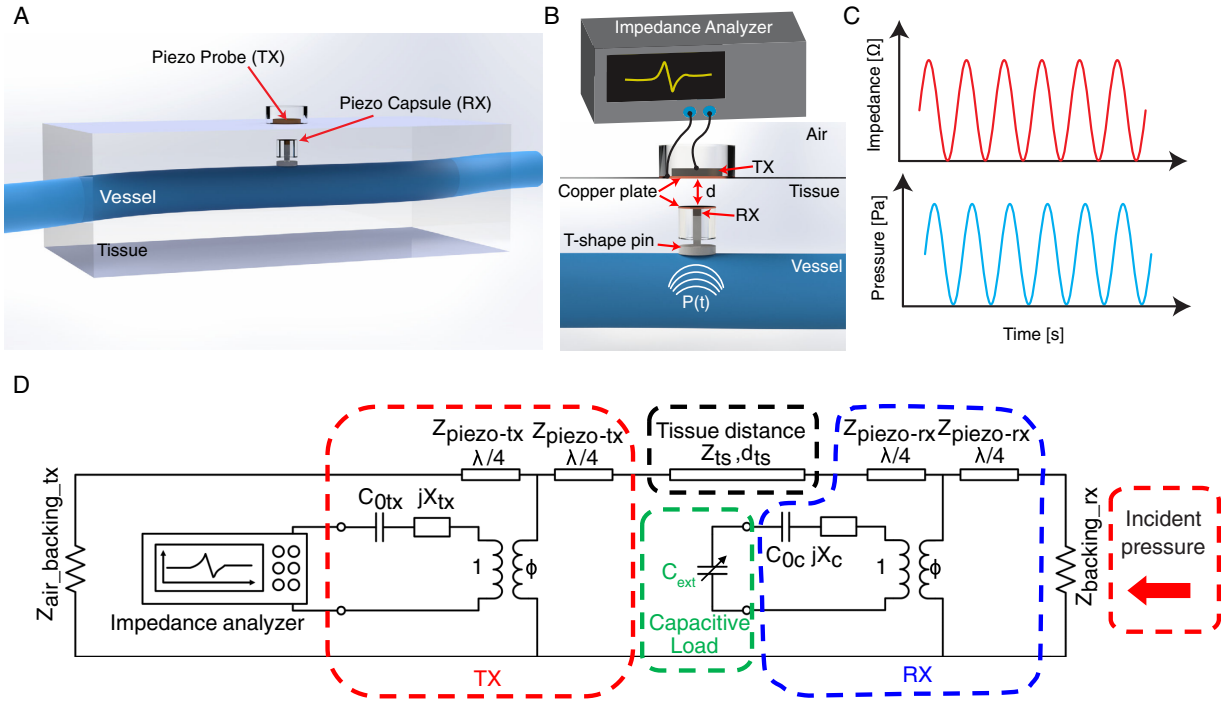


Figure 1. Ultrasonic pressure measurement concept. A) The 3D schematics of the experimental setup with the transmitter (TX) and receiver (RX) piezoelectric elements are separated by tissue-like material. The Receiver piezo capsule is attached to the outside of a pulsating vessel. B) The close-up image of ultrasound pressure measurement setup, with impedance analyzer for sending and receiving the signal through the piezo probe (TX). The piezo capsule is composed of a T-shaped pin coupled to the piezo cube (RX) to amplify the mechanical transmittance of the vessel pressure. C) The sample waveforms of the impedance (Ω) versus time that follows the pressure (Pa) profile of the pulsating vessel. D) The equivalent circuit model of the electromechanical system, consisting of the impedance analyzer, the piezo probe (TX), the piezo capsule (RX), tissue, and the incident pressure input.

changes when there is a change in the loading (mechanical or electrical) of RX. For instance, if there is a pressure change transmitted upon RX (Figure 1B) due to a pulsating flow in a vessel, the impedance analyzer can sense it in real time. Figure 1C shows a typical waveform of TX impedance at a specific frequency which follows the varying pressure profile at RX's site with time. This allows us to wirelessly measure any mechanical/electrical loading at the embedded location of the piezo capsule.

Extensive studies on ultrasonic wireless power transfer have already given the tools to analyze and design ultrasonically coupled piezoelectric transducers. Equivalent circuits for elementary piezoelectric transducers connected to the center of an acoustic transmission line have been introduced.[48] Optimal electrical load calculations have been made using the Krimholtz–Leedom–Matthaei (KLM) model to maximize ultrasonic energy transfer.[49,50] Details of ultrasonic transcutaneous energy transfer to power implanted devices have been investigated using PZT discs.[12] The equivalent electrical circuit of the TX-Tissue-RX system is depicted in Figure 1D, where the input load is reflected upon the piezo capsule (RX) and measured via the impedance analyzer of the interrogating probe (TX).

We used off-the-shelf PZT material for the piezo capsule design. The main advantage of PZT over other piezo materials is its high piezoelectric coefficient which leads to higher performance. Even though polyvinylidene fluoride (PVDF) and single-crystal lithium niobite (LiNbO3) are preferred for large aperture transducers because of their low dielectric permittivity,[41] PZT is popular because it has better sensitivity, thermal operation range, loss tangent and electromechanical coupling coefficient, which is critical to the link efficiency, compared to other piezoelectric materials. The electromechanical coupling coefficient is a figure of merit that describes the ability of the piezoelectric material to do conversion between electrical and acoustic energies.[10] However, the lead content of PZT may raise concerns in clinical trials. To avoid this, it can be encapsulated. On the other hand, biocompatible piezoelectric materials exist with properties similar but inferior to PZT. These include aluminum nitride (AlN), zinc oxide (ZnO), and barium titanate ($BaTiO_3$). Piezoelectric coefficients of AlN and ZnO are 10% of $BaTiO_3$. Therefore, $BaTiO_3$ transducers can be alternative.[41] When used in place of PZT, however, it causes a reduction in acoustic power conversion of ≈27%.[10]

To understand and characterize the proposed ultrasonically coupled system, we have first analyzed the impedance waveform in the frequency domain in hard and soft coupling media. Then, we have demonstrated a wireless pressure sensing of a pulsating vessel, emulating the artery pressure in different flow and pulse rates, which are explained in the following section.

2.2. Ultrasonic Coupling of Piezoelectric Transducers Through Hard Media

To understand the acoustic coupling between TX and RX through a hard medium, we bonded the piezoelectric

© 2022 The Authors. Advanced Intelligent Systems published by Wiley-VCH GmbH

26404567, 2022, 10, Downloaded from https://onlinelibrary.wiley.com/doi/10.1002/aisy.202200125 by Koc University, Wiley Online Library on [03/11/2022]. See the Terms and Conditions (https://onlinelibrary.wiley.com/terms-and-conditions) on Wiley Online Library for rules of use; OA articles are governed by the applicable Creative Commons License

transducers with central axis alignment to opposite sides of a plexiglass substrate (10 mm thickness), shown in **Figure 2**A. The target RX (1 mm cube) was connected to a varying capacitive load, whereas the TX (6.5 mm diameter) was connected to an impedance analyzer. We constructed an equivalent acoustic coupling system in a finite element software (COMSOL) to numerically obtain the acoustic pressure between TX, RX, and the medium. Figure 2B shows the acoustic pressure field generated at the cross-section of the medium upon excitation frequency of 2.3 MHz and input voltage of 1 V on TX. The acoustic waves generated by the piezo transducer TX could penetrate deep enough to reach RX (≈1 cm distance), enabling remote ultrasonic communication. To monitor the communicating signals, we used an impedance analyzer to measure the frequency-dependent impedance amplitude of TX. Figure 2C shows the frequency response impedance amplitude of TX when the RX was electrically connected to a range of capacitive loads. As the remote 1 mm^3 PZT cube was loaded with different capacitive loads, the impedance of the interrogator was measured using an impedance analyzer, e.g., as the load changed from 6 to 12 pF, impedance change of 2.5 Ω was measured at 2.254 MHz on the interrogating piezo site. The change in the impedance amplitude is especially large close to the resonant frequencies of the transducers, the frequency at which the maximum acoustic energy is transferred. Note that the electrical load on RX can alter the incident acoustic waves generated by TX. Figure 2D depicts the acoustic pressure change on the x-axis of the top RX surface (which is bonded to the medium) for varying capacitive loads. This change in the acoustic pressure then leads to the change in the impedance waveform of TX. The maximum change of the impedance amplitude $\Delta|Z|$ to different electrical loads can reach almost 10 Ω, as experimentally shown for a selected

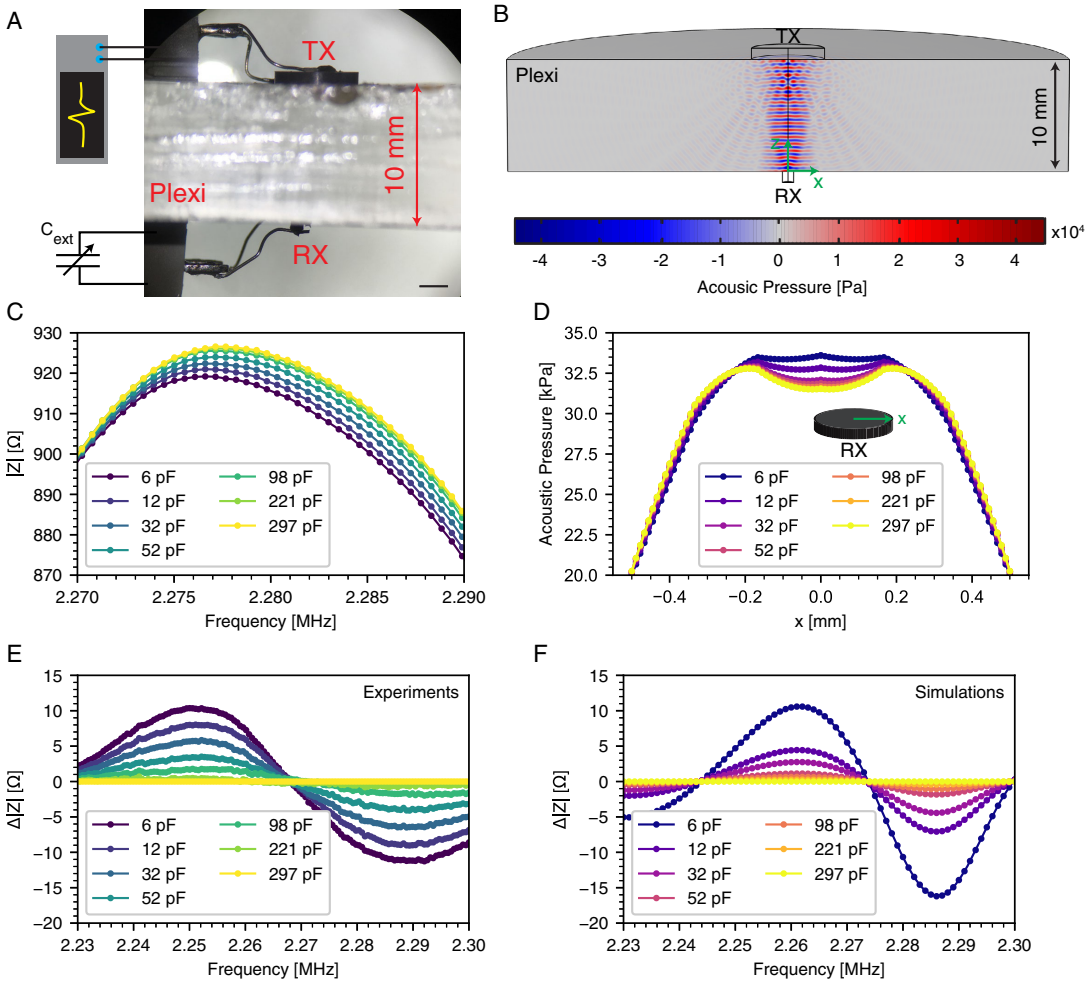


Figure 2. Characterization of wireless impedance sensing of a receiver piezo element (RX) through a hard-solid medium. A) The experiment photo shows the coupling of the TX and RX elements to 10 mm thick plexiglass medium. The TX is connected to the impedance analyzer unit and the RX is connected to a variable external capacitor. Scale bar: 1 mm. B) The finite-element (FE) simulations of the acoustic pressure generated by TX and coupled to RX through a plexiglass medium, where the blue-red color bar indicates the acoustic pressure values. C) The measured frequency response of the impedance of the TX for a range of external capacitive loads connected to the RX. D) The simulation results of the radius-dependent acoustic pressure of RX at its intersection with the coupling medium for a range of external capacitive loads. The pressure change due to the varying capacitance is maximum at the center of the RX. E–F) The experimental results and numerical simulations of the TX impedance change compared to the highest capacitive load.

© 2022 The Authors. Advanced Intelligent Systems published by Wiley-VCH GmbH

26404567, 2022, 10, Downloaded from https://onlinelibrary.wiley.com/doi/10.1002/aisy.202200125 by Koc University, Wiley Online Library on [03/11/2022]. See the Terms and Conditions (https://onlinelibrary.wiley.com/terms-and-conditions) on Wiley Online Library for rules of use; OA articles are governed by the applicable Creative Commons License

frequency range in Figure 2E. For a similar frequency range, the simulations can capture the similar impedance change, shown in Figure 2F.

2.3. Ultrasonic Coupling of Piezoelectric Transducers Through Soft Media

The speed of sound in soft media such as lossy PDMS or biological tissues is much different from that in the hard medium. To characterize the acoustic coupling in soft media between TX and RX, we performed experiments on a PDMS and a chicken breast, as shown in **Figure 3**A,B. Unlike the previous section with permanent bonding of TX and RX to the hard medium, we used ultrasound gel for coupling the piezo transducers to the soft medium. When the center axes of TX and RX were aligned, we could observe the change in the TX impedance amplitude, while changing the electrical load at RX. Figure 3C shows the impedance change curves ($\Delta|Z|$ as they are compared to the highest capacitive load $C_{ext} = 556$ pF as the reference capacitor) for a range of electrical loads within a frequency range of 2–2.35 MHz. The bottom panel in Figure 3C shows the absolute impedance amplitude of TX at the gray shaded frequency region of the top panel. The increasing trend of capacitive loads at the RX was reflected by the decreasing trend of absolute impedance amplitude of TX. We performed a similar set of experiments using the 1 cm-thick chicken breast as the coupling medium. Figure 3D depicts the impedance change ($\Delta|Z|$ compared to the highest capacitive load $C_{ext} = 556$ pF as the reference capacitor) and absolute impedance values for a shaded frequency range. The maximum change in the impedance values was considerably higher in the chicken breast medium than that in the PDMS slab. Across 4 mm thick PDMS, 0.2 Ω impedance change was measured as a capacitive load of the miniature piezo cube changed from 2.7 to 8.7 pF at 2.315 MHz. On the other hand, 0.5 Ω change was measured with 1 cm thick chicken breast tissue as capacitive load increased from 6.4 to 13 pF at 2.265 MHz. This clearly shows the effect of acoustic pressure wave attenuation in the lossy PDMS medium as discussed in the previous studies;[51] whereas, the chicken tissue, composed mostly of water, can transmit acoustic waves with lower acoustic wave damping.

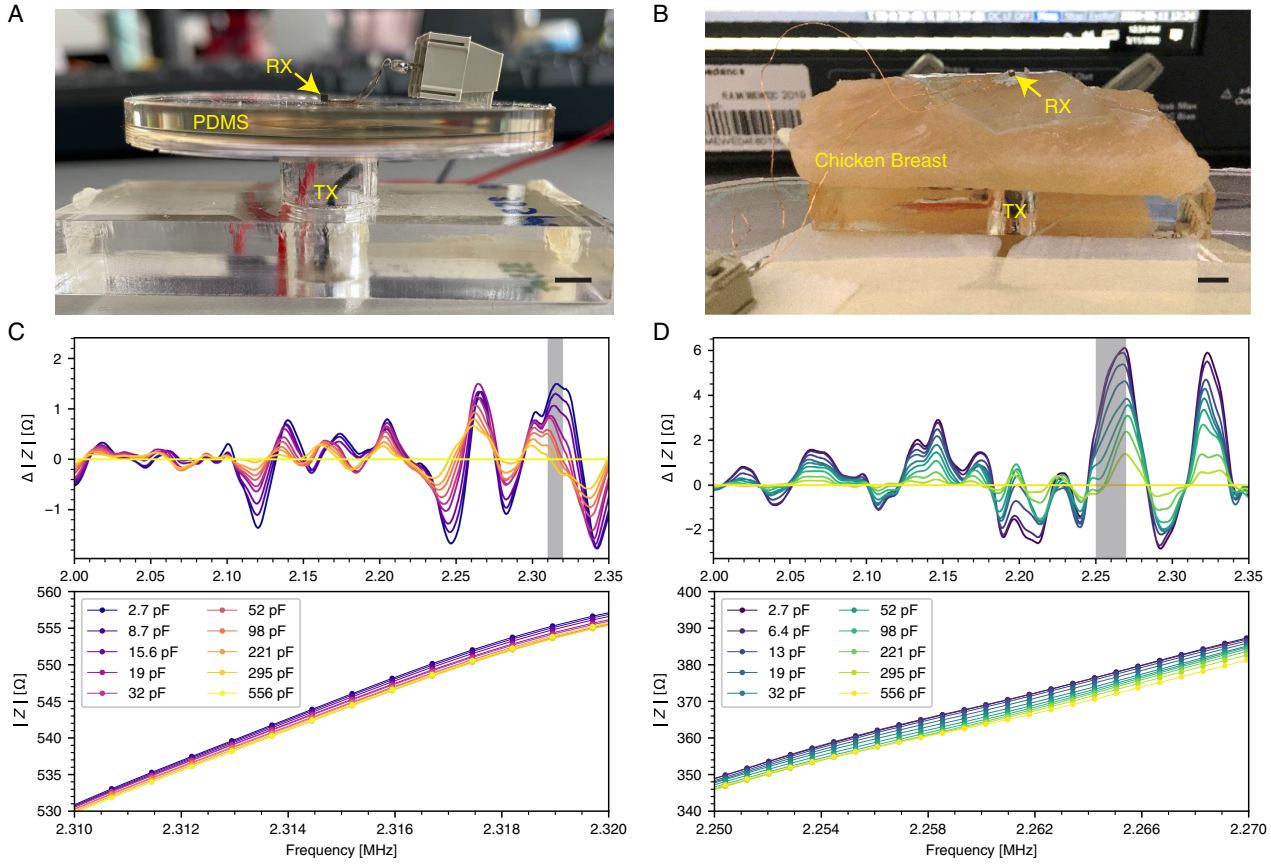


Figure 3. Characterization of wireless impedance sensing of a receiver piezo element (RX) through a soft-solid medium. A) The transmitter piezo TX is coupled to a 4 mm thick polydimethylsiloxane (PDMS) medium, and aligned with the receiver piezo RX which is connected to an external capacitance and placed on the other side of the medium. Both piezo elements are coupled to the medium via ultrasound gel. Scale bar, 5 mm B) A chicken breast is used as a biological medium between TX and RX. Scale bar, 5 mm. C) The frequency-dependent impedance change curve of PDMS medium for a range of capacitive loads that are compared to the highest capacitive load Cp = 556 pF (top). The impendance sensitivity curve of the gray-shaded frequency range (bottom). D) The frequency-dependent impedance change curve of chicken breast medium for a range of capacitive loads that are compared to the highest capacitive load Cp = 556 pF (top). The impendance sensitivity curve of the gray-shaded frequency range (bottom).

© 2022 The Authors. Advanced Intelligent Systems published by Wiley-VCH GmbH

26404567, 2022, 10, Downloaded from https://onlinelibrary.wiley.com/doi/10.1002/aisy.202200125 by Koc University, Wiley Online Library on [03/11/2022]. See the Terms and Conditions (https://onlinelibrary.wiley.com/terms-and-conditions) on Wiley Online Library for rules of use; OA articles are governed by the applicable Creative Commons License

2.4. Wireless Pressure Measurements with Piezo Capsule Design

After investigating the acoustic coupling mechanism in hard and soft media between TX and RX, we implanted the piezo capsule in the artificial vessel with the pulsating flow, akin to pulsating blood flow in the artery. **Figure 4**A,B shows the complete experimental setup, including the pulsatile pump, tubes, reference wired pressure sensor, piezo cube (RX) as part of the piezo capsule, piezo probe (TX), and impedance analyzer. We implanted the piezo capsule on the outer surface of the vessel and covered it with PDMS to resemble tissue-like surroundings. The mechanical T-shaped design (Figure 4A, inset) enables a mechanical pressure amplification from the incident pressure, at the larger area side of the pin in contact with the vessel wall, to the piezoelectric surface at the lower area side. The rigidity of PMMA enables lossless transmission of force, therefore the applied pressure to the piezoelectric surface is dependent on the larger area (A_1) to smaller area (A_2) ratio, i.e., $P_2 = P_1 \times (A_1/A_2)$. This way, we could enhance the sensitivity of the pressure reading, by simply increasing the pin area (to 3 mm in diameter), which is in contact with the vessel wall.

We aligned TX to RX across a 7 mm distance along the center axis where its coupling to the PDMS surface was achieved via ultrasound gel. To measure the true pulsating pressure inside the vessel, we employed a resistive pressure sensor for recording the pressure profile in time. By varying the pump's pulse frequency of the flow at a constant volume, we could observe the pulsatile pressure behavior inside the vessel. At the same time, the impedance amplitude of TX could capture the pulsatile flow behavior of the vessel wirelessly, as shown in Figure 4C. The increasing pulsatile frequency led to an increase in pressure

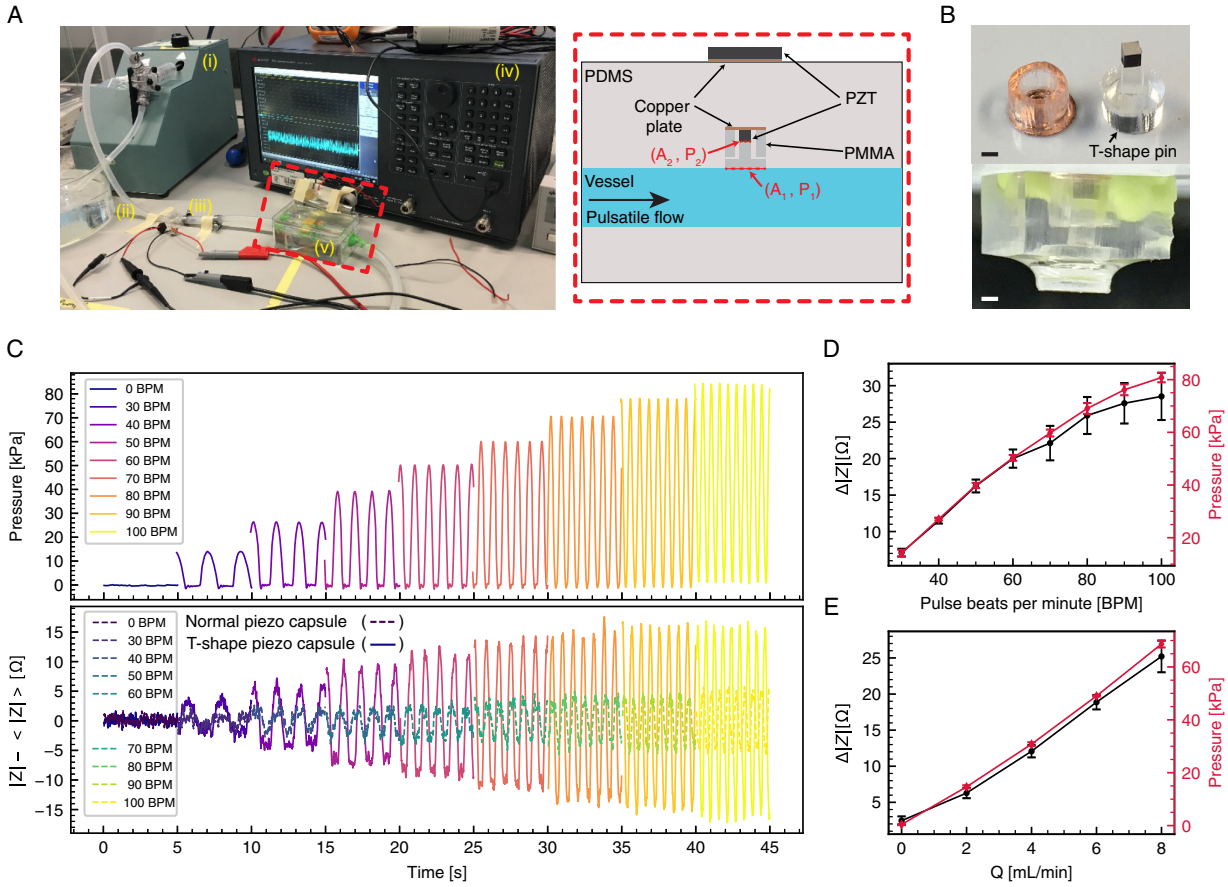


Figure 4. Wireless monitoring of pulsating pressure in a vessel-like tube. A) The experimental setup for the transient impedance measurement of the piezo TX, consisting of: i) pulsatile pump, ii) the 6 mm diameter tube, iii) embedded pressure sensor, iv) the impedance analyzer unit, v) piezo TX, PDMS-filled container, and embedded piezo cube RX across 7 mm distance. (inset) The cross-section of the piezo capsule mounted on the vessel wall is shown. The larger area A_1 of the T-shaped pin experiences pressure P_1 (red arrow), and the smaller area A_2 of the pin gives higher pressure P_2 to the piezo cube surface (red arrow) B) The close-up images of the piezo capsule, piezo cube RX and the T-shaped pin. The diameter and length of the pin are equally 3 mm. Scale bar: 1 mm C) The transient impedance change curve for varying pulsating pressure (bottom), correlated to the pressure curve of the tube measured by the embedded pressure sensor (top). The impedance change accurately follows the pulsating pressure of the tube. The bottom impedance curve also shows the ×3.2 improvement of the piezo capsule design with a T-shaped pin compared to the response of a single piezo cube RX. D) The sensitivity curves of the impedance change (Ω) and pressure (kPa) versus the fluid pulse frequency (bpm). E) The sensitivity curves of the impedance change (Ω) and pressure (kPa) versus the volumetric flow rate (mL min^{-1}). The error bars represent the standard deviation of three independent measurements.

© 2022 The Authors. Advanced Intelligent Systems published by Wiley-VCH GmbH

26404567, 2022, 10, Downloaded from https://onlinelibrary.wiley.com/doi/10.1002/aisy.202200125 by Koc University, Wiley Online Library on [03/11/2022]. See the Terms and Conditions (https://onlinelibrary.wiley.com/terms-and-conditions) on Wiley Online Library for rules of use; OA articles are governed by the applicable Creative Commons License

amplitude, which was accurately captured by both the reference wired pressure sensor and the wireless piezo capsule. The sensitivity curves of the impedance change (Ω), hence pressure (kPa), versus the fluid pulse frequency (bpm) and the volumetric flow rate ($mL\,min^{-1}$) are measured. Figure 4D summarizes the sensitivity of impedance amplitude and pressure amplitude to varying flow pulse frequencies between 30 and 100 bpm. The sensitivity of $0.375\,\Omega\,kPa^{-1}$ was achieved in the pressure range from 14 to 86 kPa as pulse frequency changed from 30 to 100 bpm with a fixed flow rate of $8\,mL\,min^{-1}$. Impedance change of 32 Ω was measured as $8\,mL\,min^{-1}$ flow rate was pulsed at 100 bpm. This shows a factor of 3.2 improvements with smart capsule design compared to having just a single piezoelectric transducer as evident from the results of Figure 4C bottom panel. In both cases, the distance of the piezo RX to the piezo TX was the same. At high-pressure amplitudes, we observed a larger variation in the impedance amplitude values; which could be attributed to the nonlinear deformation of the vessel wall at high pulse frequencies. We also investigated the effect of the volumetric rate of the fluid flow on the vessel wall pressure at a constant pulse frequency of 80 bpm. Figure 4E shows the sensitivity of impedance amplitude and pressure amplitude to the varying volumetric flow rates. The same sensitivity of $0.375\,\Omega\,kPa^{-1}$ was measured and 22.5 Ω impedance change was recorded as the flow rate increased from 0 to $8\,mL\,min^{-1}$. The repeated experiments indicate the robustness of the measurements at different volumetric flow rates, although a larger deviation in the impedance amplitude was observed at high-pressure amplitudes. Overall, wireless pressure measurements via coupling of TX and the embedded piezo capsule have shown promising results for real-time vessel wall pressure monitoring.

3. Discussions

We demonstrated the ultrasonic pressure measurements of vessels using a piezo capsule, and an interrogating piezoelectric probe. We first showed that by ultrasonic communication between TX and RX, an electrical loading effect (e.g., the external capacitive load on RX) can be detected through hard and soft media. The monitoring of electrical load change at the target RX is the most sensitive at the resonant frequencies of the piezoelectric transducers, which can be captured by an impedance analyzer without requiring any special circuitry. Besides monitoring the static changes at the target point, we showed the dynamic pressure reading capabilities of the piezoelectric capsule design. Emulating the pulsatile fluidic flow at different volumetric rates, we were able to remotely detect the dynamic pressure profile in real time. The impedance change for various flow parameters was validated by the reference pressure sensor, which proves the viability of the proposed ultrasonic pressure monitoring approach. Last, through the integration of a simple, passive T-shaped mechanical structure, we showed a drastic enhancement in the sensitivity of pressure reading (3.2 times improvement in the impedance amplitude), which was attributed to increased mechanical loading to the piezo cube.

The potential use of the proposed battery-less, passive piezoelectric capsule implant could be in long-term cardiac pressure monitoring. After complying with the biocompatibility and non-toxicity guidelines, the packaged piezo capsule could be attached around the vessel by a ring or an adhesive, where the wall pressure is applied to the piezo surface. Besides, the proposed piezo capsules could be used in a wide range of industrial applications that are involved with pressure monitoring in harsh environments; for example, they could be implanted inside pipes to read the varying pressure of gas/liquid flow.

We should note that all piezoelectric materials are lossy for long-term DC pressure measurements as piezoelectric charges decay gradually with time. The usage of piezoelectric resonators in the thickness mode can alleviate this problem. A pressure sensor based on the piezoelectric resonance of poly(vinylidene fluoride-trifluoroethylene) (P(VDF-TrFE)) has already been shown to avoid long-term drift from the charge leakage problem in quasi-static pressures and integrated into RF circuits for wireless operation using RF backscattering.[52] An alternative solution to long-term static pressure value readings could be via capacitive sensors (e.g., MEMS capacitive sensors[32]) that can electrically load the piezo capsule, and hence change the interrogating piezoelectric probe's impedance value close to its resonance frequency.

Future work will explore the usage of ultrasonic beamforming with a phased array to improve tolerance to misalignment and enable multiple piezo capsule readings from different locations.[11,53] The array of piezo capsules, distributed along the vessel walls, could provide spatial pressure information and reduce the signal noise experienced by a single sensor.

4. Experimental Section

Fabrication of the Piezoelectric Capsule and Ultrasound Probe: The piezoelectric capsule was composed of 1 mm×1 mm×1 mm PZT cube (PIC 181, PI Ceramic GmbH), bonded from one side on a 100 μm thick copper substrate, and from the opposite side attached to a laser-cut plexiglass T-shaped structure. The custom-made ultrasound probe was fabricated using a 6.5 mm × 1 mm PZT disk (PIC 181, PI Ceramic GmbH) bonded on a 100 μm thick copper substrate and two cables were connected to opposite electrodes of PZT using an electrically conductive epoxy (EPO-TEK H20E-PFC, Epoxy Technology). A laser-cut plexiglass housing was also glued to the copper substrate for facilitating probe handling.

Impedance Signal Recording and Pressure Measurements: The impedance of the ultrasound probe in the frequency domain was measured using a vector network analyzer (E5061B, Keysight Technologies). The pulsatile flow with controllable pulse frequency and the volumetric flow rate was provided using a pulsatile blood pump (Harvard Apparatus). For reference pressure measurement inside the artificial vessel, a piezoresistive silicon micromachined absolute pressure sensor (MS5401-BM, TE Connectivity Measurement Specialties, Inc.) was used. The electrical signals from the pressure sensor were recorded by an oscilloscope and later analyzed in Python.

Numerical Finite Element Analysis: COMSOL Multiphysics 5.6 (COMSOL Inc.) was used to obtain the pressure field and impedance amplitude of the piezoelectric probe. The physics modules of acoustic structure and piezoelectric effect were used to model the propagation of acoustic waves from the oscillating piezoelectric element to the coupling medium (e.g., plexiglass). Then, the electrical circuit physics was used to obtain the electrical impedance of the ultrasound probe (TX) while the target piezo cube (RX) was connected to a varying capacitive load. All simulations were conducted in the frequency domain.

Statistical Analysis: Experimental results represent the mean ± standard deviation of the measurements.

© 2022 The Authors. Advanced Intelligent Systems published by Wiley-VCH GmbH

26404567, 2022, 10, Downloaded from https://onlinelibrary.wiley.com/doi/10.1002/aisy.202200125 by Koc University, Wiley Online Library on [03/11/2022]. See the Terms and Conditions (https://onlinelibrary.wiley.com/terms-and-conditions) on Wiley Online Library for rules of use; OA articles are governed by the applicable Creative Commons License

Acknowledgements

S.M. and A.A. contributed equally to this work. This work is funded by the Max Planck Society.

Open Access funding enabled and organized by Projekt DEAL.

Conflict of Interest

The authors declare no conflict of interest.

Author Contributions

S.M. and A.A.: conceived and coordinated the project. M.S.: supervised the research. S.M., A.A., and M.S.: wrote and edited the manuscript.

Data Availability Statement

The data that support the findings of this study are available from the corresponding author upon reasonable request.

Keywords

piezoelectric, ultrasonic coupling, ultrasonic implant, ultrasound pressure sensor, wireless pressure reading

Received: May 12, 2022
Revised: June 27, 2022
Published online: August 10, 2022

[1] G. Savarese, L. H. Lund, *Cardiac Fail. Rev.* **2017**, *3*, 7.
[2] E. Y. Chow, A. L. Chlebowski, S. Chakraborty, W. J. Chappell, P. P. Irazoqui, *IEEE Trans. Biomed. Eng.* **2010**, *57*, 1487.
[3] R. L. Hammond, K. Hanna, C. Morgan, P. Perakis, N. Najafi, G. W. Long, C. J. Shanley, *Asaio J.* **2012**, *58*, 83.
[4] S. Mutlu, in *Somatosensory Feedback for Neuroprosthetics*, Elsevier, Amsterdam **2021**, pp. 537.
[5] K. D. Wise, D. J. Anderson, J. F. Hetke, D. R. Kipke, K. Najafi, *Proc. IEEE* **2004**, *92*, 76.
[6] J. A. Potkay, *Biomed. Microdevices* **2008**, *10*, 379.
[7] S. A. Mirbozorgi, P. Yeon, M. Ghovanloo, *IEEE Trans. Biomed. Circuits Syst.* **2017**, *11*, 692.
[8] V. K. Bandari, Y. Nan, D. Karnaushenko, Y. Hong, B. Sun, F. Striggow, D. D. Karnaushenko, C. Becker, M. Faghih, M. Medina-Sánchez, F. Zhu, O. G. Schmidt, *Nat. Electron.* **2020**, *3*, 172.
[9] A. D. Dehennis, K. D. Wise, *J. Microelectromech. Syst.* **2005**, *14*, 12.
[10] D. K. Piech, B. C. Johnson, K. Shen, M. M. Ghanbari, K. Y. Li, R. M. Neely, J. E. Kay, J. M. Carmena, M. M. Maharbiz, R. Muller, *Nat. Biomed. Eng.* **2020**, *4*, 207.
[11] A. Arbabian, T. C. Chang, M. L. Wang, J. Charthad, S. Baltsavias, M. Fallahpour, M. J. Weber, *IEEE Microwave Mag.* **2016**, *17*, 39.
[12] S. Ozeri, D. Shmilovitz, *Ultrasonics* **2010**, *50*, 556.
[13] M. Han, H. Wang, Y. Yang, C. Liang, W. Bai, Z. Yan, H. Li, Y. Xue, X. Wang, B. Akar, H. Zhao, H. Luan, J. Lim, I. Kandela, G. A. Ameer, Y. Zhang, Y. Huang, J. A. Rogers, *Nat. Electron.* **2019**, *2*, 26.
[14] C. Shi, T. Costa, J. Elloian, Y. Zhang, K. L. Shepard, *IEEE Trans. Biomed. Circuits Syst.* **2020**, *14*, 412.
[15] Y. Lee, S. Bang, I. Lee, Y. Kim, G. Kim, M. H. Ghaed, P. Pannuto, P. Dutta, D. Sylvester, D. Blaauw, *IEEE J. Solid-State Circuits* **2012**, *48*, 229.
[16] I. Haydaroglu, M. T. Ozgun, S. Mutlu, *IEEE Trans. Circuits and Syst. I: Regul. Pap.* **2017**, *64*, 2003.
[17] X. Wu, I. Lee, Q. Dong, K. Yang, D. Kim, J. Wang, Y. Peng, Y. Zhang, M. Saligane, M. Yasuda, K. Kumeno, F. Ohno, S. Miyoshi, M. Kawaminami, D. Sylvester, D. Blaauw, in *2018 IEEE Symposium on VLSI Circuits*, IEEE, Piscataway,NJ pp.191–192.
[18] E. O. Torres, G. A. Rincón-Mora, *IEEE Trans. Circuits Syst. I: Regul. Pap.* **2008**, *56*, 1938.
[19] J. Zhong, Z. Li, M. Takakuwa, D. Inoue, D. Hashizume, Z. Jiang, Y. Shi, L. Ou, M. Osman, G. Nayeem, S. Umezu, K. Fukuda, T. Someya, *Adv. Mater.* **2022**, *34*, 2107758.
[20] S. P. Beeby, R. N. Torah, M. J. Tudor, P. Glynne-Jones, T. O'Donnell, C. R. Saha, S. Roy, *J. Micromech. Microeng.* **2007**, *17*, 1257.
[21] S. D. Moss, O. R. Payne, G. A. Hart, C. Ung, *Smart Mater. Struct.* **2015**, *24*, 023001.
[22] A. Pfenniger, L. N. Wickramarathna, R. Vogel, V. M. Koch, *Med. Eng. Phys.* **2013**, *35*, 1256.
[23] H. Kulah, K. Najafi, *IEEE Sens. J.* **2008**, *8*, 261.
[24] Y. K. Ramadass, A. P. Chandrakasan, *IEEE J. Solid-State Circuits* **2010**, *46*, 333.
[25] S. Mutlu, K. Unlu, T. N. Gevrek, A. Sanyal, *Smart Mater. Struct.* **2020**.
[26] Y. Ma, Q. Zheng, Y. Liu, B. Shi, X. Xue, W. Ji, Z. Liu, Y. Jin, Y. Zou, Z. An, W. Zhang, X Wang, W. Jiang, Z. Xu, Z. L. Wang, Z. Li, H. Zhang, *Nano Lett.* **2016**, *16*, 6042.
[27] I. Kara, M. Becermis, M. Abdel-Aal Kamar, M. Aktan, H. Dogan, S. Mutlu, *IEEE Trans. Circuits Syst. I: Regul. Pap.* **2020**, *68*, 210.
[28] H. Ouyang, Z. Li, M. Gu, Y. Hu, L. Xu, D. Jiang, S. Cheng, Y. Zou, Y. Deng, B. Shi, W. Hua, Y. Fan, Z. Li, Z. Wang, *Adv. Mater.* **2021**, *33*, 2102302.
[29] H. Ahn, B. Delshad, J. Baranowski, *J. Cardiovasc. Dis. Dia.* **2016**, *4*, 252.
[30] M. G. Allen, in *The 13th Int. Conf. on Solid-State Sensors, Actuators and Microsystems, 2005. Digest of Technical Papers. TRANSDUCERS'05*, Seoul, Korea (South) pp. 275–278.
[31] C. M. Boutry, L. Beker, Y. Kaizawa, C. Vassos, H. Tran, A. C. Hinckley, R. Pfattner, S. Niu, J. Li, J. Claverie, Z. Wang, J. Chang, P. M. Fox, Z. Bao, *Nat. Biomed. Eng.* **2019**, *3*, 47.
[32] M. S. Arefin, J.-M. Redouté, M. R. Yuce, *IEEE J. Biomed. Health Inf.* **2017**, *22*, 87.
[33] O. H. Murphy, M. R. Bahmanyar, A. Borghi, C. N. McLeod, M. Navaratnarajah, M. H. Yacoub, C. Toumazou, *Biomed. Microdevices* **2013**, *15*, 737.
[34] D. M. Shavelle, A. S. Desai, W. T. Abraham, R. C. Bourge, N. Raval, L. D. Rathman, J. T. Heywood, R. A. Jermyn, J. Pelzel, O. T. Jonsson, M. R. Costanzo, J. D. Henderson, M.-E. Brett, P. B. Adamson, L. W. Stevenson, CardioMEMS Post-Approval Study Investigators, *Circ. Heart Fail.* **2020**, *13*, 006863.
[35] K. S. Rao, P. V. Nikitin, S. F. Lam, *IEEE Trans. Antennas Propag.* **2005**, *53*, 3870.
[36] B. W. Cook, S. Lanzisera, K. S. Pister, *Proc. IEEE* **2006**, *94*, 1177.
[37] W. Biederman, D. J. Yeager, N. Narevsky, A. C. Koralek, J. M. Carmena, E. Alon, J. M. Rabaey, *IEEE Journal of Solid-State Circuits* **2013**, *48*, 960.
[38] S. O'Driscoll, A. S. Poon, T. H. Meng, in *2009 IEEE International Solid-State Circuits Conference-Digest of Technical Papers*, IEEE, Piscataway, NJ, pp. 294.
[39] M. M. Maharbiz, R. Muller, E. Alon, J. M. Rabaey, J. M. Carmena, *Proc. IEEE* **2016**, *105*, 73.
[40] IEEE Standards Coordinating Committee, IEEE standard for safety levels with respect to human exposure to radio frequency electromagnetic fields, 3kHz to 300GHz. IEEE C95. 1-2005, **2005**.

© 2022 The Authors. Advanced Intelligent Systems published by Wiley-VCH GmbH

26404567, 2022, 10, Downloaded from https://onlinelibrary.wiley.com/doi/10.1002/aisy.202200125 by Koc University, Wiley Online Library on [03/11/2022]. See the Terms and Conditions (https://onlinelibrary.wiley.com/terms-and-conditions) on Wiley Online Library for rules of use; OA articles are governed by the applicable Creative Commons License

[41] D. Seo, J. M. Carmena, J. M. Rabaey, E. Alon, M. M. Maharbiz, arXiv preprint arXiv:1307.2196 **2013**.
[42] Administration, F. A. D., Guidance for industry and FDA staff information for manufacturers seeking marketing clearance of diagnostic ultrasound systems and transducers, FDA, Rockville, MD, **2017**.
[43] D. Seo, R. M. Neely, K. Shen, U. Singhal, E. Alon, J. M. Rabaey, J. M. Carmena, M. M. Maharbiz, *Neuron* **2016**, *91*, 529.
[44] M. J. Weber, Y. Yoshihara, A. Sawaby, J. Charthad, T. C. Chang, A. Arbabian, *IEEE J. Solid-State Circuits* **2018**, *53*, 1089.
[45] T. C. Chang, M. J. Weber, J. Charthad, S. Baltsavias, A. Arbabian, *IEEE Trans. Biomed. Circuits Syst.* **2018**, *12*, 1100.
[46] T. Fan, Z. Liu, Z. Luo, J. Li, X. Tian, Y. Chen, Y. Feng, C. Wang, H. Bi, X. Li, F. Qiao, X. Wu, *Adv. Intell. Syst.* **2021**, *3*, 2000184.
[47] G. Chen, S. Hanson, D. Blaauw, D. Sylvester, *Proc. IEEE* **2010**, *98*, 1808.
[48] R. Krimholtz, D. A. Leedom, G. L. Matthaei, *Electron. Lett.* **1970**, *6*, 398.
[49] M. Gorostiaga, M. Wapler, U. Wallrabe, in *2016 IEEE International Ultrasonics Symposium (IUS)*, IEEE, Piscataway, NJ, pp. 1–4.
[50] S. Van Kervel, J. Thijssen, *Ultrasonics* **1983**, *21*, 134.
[51] A. Aghakhani, A. Pena-Francesch, U. Bozuyuk, H. Cetin, P. Wrede, M. Sitti, *Sci. Adv.* **2022**, *8*, eabm5126.
[52] X. Li, E. C. Kan, *Sens. Actuators A: Phys.* **2010**, *163*, 457.
[53] D. Seo, H.-Y. Tang, J. M. Carmena, J. M. Rabaey, E. Alon, B. E. Boser, M. M. Maharbiz, in *2015 37th Annual Int. Conf. of the IEEE Engineering in Medicine and Biology Society (EMBC)*, IEEE, Piscataway, NJ pp. 2673–2676.

© 2022 The Authors. Advanced Intelligent Systems published by Wiley-VCH GmbH

26404567, 2022, 10, Downloaded from https://onlinelibrary.wiley.com/doi/10.1002/aisy.202200125 by Koc University, Wiley Online Library on [03/11/2022]. See the Terms and Conditions (https://onlinelibrary.wiley.com/terms-and-conditions) on Wiley Online Library for rules of use; OA articles are governed by the applicable Creative Commons License